Journal of Nuclear Medicine, published on April 26, 2019 as doi:10.2967/jnumed.118.225250

Radiation dosimetry and biodistribution of ^{18}F-PSMA-11 for PET imaging of prostate cancer

Sarah Piron[1], Kathia De Man[2], Nick Van Laeken[2], Yves D'Asseler[2], Klaus Bacher[3], Ken Kersemans[2], Piet Ost[4], Karel Decaestecker[5], Pieter Deseyne[4], Valérie Fonteyne[4], Nicolaas Lumen[5], Eric Achten[2], Boudewijn Brans[2], Filip De Vos[1]

[1] Ghent University, Laboratory of Radiopharmacy, Ghent, Belgium

[2] Ghent University Hospital, Dept Nuclear Medicine, Ghent, Belgium

[3] Ghent University Hospital, Dept of Human Structure and Repair, Ghent, Belgium

[4] Ghent University Hospital, Dept Radiation Oncology, Ghent, Belgium

[5] Ghent University Hospital, Dept Urology, Ghent, Belgium

First author and responsible for correspondence:

Sarah Piron

Ottergemsesteenweg 460, 9000 Ghent

BE-Belgium

0032 9 264 8045

sarah.piron@ugent.be

PhD student

Running title: ^{18}F-PSMA-11 PET/CT for prostate cancer

Keywords: dosimetry, PSMA, ^{18}F-PSMA-11, PET/CT, prostate cancer

Word count: 5043

ABSTRACT

Prostate specific membrane antigen (PSMA) is highly overexpressed in prostate cancer. Many PSMA analogue radiotracers for PET/CT imaging of prostate cancer staging have been developed such as ^{68}Ga-PSMA-11. This radiotracer has achieved good results in multiple clinical trials, but because of superior imaging characteristics of ^{18}F-fluoride, ^{18}F-PSMA-11 was developed. The aim of this study was to evaluate the safety of administration and the radiation dosimetry of ^{18}F-PSMA-11. METHODS Six patients (age 62-68y, mean 66 ± 2y) with suspected prostate cancer recurrence after previous treatment were administered 2 MBq/kg bodyweight ^{18}F-PSMA-11 followed by PET/$CT_{low\text{-}dose}$ imaging at 0, 20, 50, 90 and 300 min post injection (p.i.). To evaluate the safety of administration, vital parameters were monitored. To assess toxicity, full blood count and biochemical parameters were determined. According to the latest ICRP recommendations, radiation dosimetry analysis was performed using IDAC-Dose 2.1. For blood activity measurement, small samples of venous blood were collected at various timepoints p.i. The unbound ^{18}F-fluoride fraction was determined in plasma 20, 50 and 90 min after administration to evaluate the defluorination rate of ^{18}F-PSMA-11. RESULTS After injection, ^{18}F-PSMA-11 was rapidly cleared from the blood. 29.0 ± 5.9% of the activity was excreted in urine at 5h p.i. The free ^{18}F fraction in plasma increased from 9.7 ± 1.0% 20 min p.i. to 22.2 ± 1.5% 90 min p.i. The highest tracer uptake was observed in kidneys, bladder, spleen and liver. No study drug related adverse events were observed. The calculated mean effective dose was 12.8 ± 0.6 µSv/MBq. CONCLUSION ^{18}F-PSMA-11 can be safely administered and results in a mean effective dose of 12.8 ± 0.6 µSv/MBq. Therefore, the total radiation dose is lower compared to other PSMA PET agents and in the same range of ^{18}F-DCFPyL.

INTRODUCTION

In men, prostate cancer is the second most frequently diagnosed cancer worldwide (*1*). A major issue in the clinical management is early detection of recurrent disease after radical prostatectomy or local therapy with curative intent. Approximately 30% of patients undergoing radical prostatectomy experience biochemical recurrence within 10 years (*2*). Usually, this recurrence first presents itself through an increased serum prostate-specific antigen (PSA) level (*3*). However, for salvage therapy to be successful, precise localization of metastases is necessary to determine the most appropriate treatment. As PSA levels make no distinction between local and systemic disease, there is a need for reliable imaging biomarkers to determine the exact location of metastatic tumours (*4*,*5*).

Limitations of currently used imaging probes have led to a growing interest in new PET tracers for improved imaging of prostate cancer metastases (*6*,*7*). Over the last few years, prostate specific membrane antigen (PSMA) has gained a lot of interest as a specific target for prostate cancer imaging. Although PSMA is also expressed in normal prostate tissue and in other organs such as small intestine, salivary glands and kidneys, the expression level in both primary and metastatic prostate cancer is 100 to 1000 fold higher (*8*–*10*).

Good results have been achieved with the recently developed radiotracer Glu-NH-CO-NH-Lys-(Ahx)-^{68}Ga-(HBED-CC) (^{68}Ga-PSMA-11) which is recommended for biochemical recurrent prostate cancer restaging (*11*–*13*). However, while ^{68}Ga as a PET isotope is beneficial for centres without a cyclotron, its use is associated with several disadvantages such as the short lifespan of

the $^{68}Ge/^{68}Ga$ generator, the limited patient doses per generator elution and short half-life. Additionally, the high positron energy of ^{68}Ga (E_{max} 1.899 MeV) contributes to the larger positron range which decreases the spatial resolution of the PET images while the low positron yield (87,7%) leads to a reduced sensitivity. This makes detection of small metastatic lesions with low PSMA expression difficult (*14*–*16*).

Therefore, there is an increased demand for the development and clinical validation of ^{18}F-labelled PSMA targeting radiotracers such as ^{18}F-DCFBC (*17*), ^{18}F-DCFPyl (*18*) and ^{18}F-PSMA-1007 (*19*). However, these radiotracers encounter disadvantages such as high blood pool activity, regional patent protection and slow excretion kinetics, respectively. To overcome these issues, ^{18}F-PSMA-11 was introduced by Malik *et al.* (*20*) and Boschi *et al.* (*21*). The precursor (PSMA-11) is readily available and a GMP compliant radiosynthesis was recently developed by Kersemans *et al.* (*14*), which allows for large scale production and implementation in clinical routine. Although the synthesis of this compound has been thoroughly investigated (*14*,*20*–*22*), no clinical data on first human administration have yet been published.

The aim of this study was to assess the safety of administration and biodistribution of ^{18}F-PSMA-11 in humans. Secondary goals included the determination of the radiotracer kinetics and metabolites in plasma and urine, the establishment of critical organs, and the calculation of the organ dosimetry and total body effective dose.

MATERIALS AND METHODS

The study was approved by the Ethics Committee of the Ghent University Hospital (2017/1294) and conducted following the International Conference on Harmonisation Good Clinical Practice E6 (R2) guidelines and the Declaration of Helsinki (EudraCT nr: 2017-003461-96). The study was supported by the Flemish foundation FWO TBM (T001517). All subjects signed a written consent before participation to the study.

Six patients (age 62-68y, median 66.5y) with biochemical recurrence after curative treatment (prostatectomy with or without lymphadenectomy or radiotherapy) were prospectively enrolled in the study during a consultation with their treating physician. Patients who were under 40 or above 70 years old, who were physically or mentally unfit to perform the planned procedures or who refused to be informed about accidental findings on scans were excluded from the study. Patient characteristics are provided in Table 1.

To evaluate the safety of ^{18}F-PSMA-11 administration, vital parameters such as body temperature, blood pressure and heart rate were measured at multiple timepoints up to 5h post injection (p.i.). To determine toxicity, full blood count was performed, as well as measurement of sodium, creatinine, alanine aminotransferase and alkaline phosphatase before and 300 min after administration of ^{18}F-PSMA-11. Adverse events were reported up to 24h p.i. according to the CTCAE 4.0 scoring system.

PET/CT imaging was performed using a GE Discovery MI 3 ring system, a digital PET/CT scanner with SiPM based PET detectors coupled to lutetium based scintillators, an axial field of view of 15 cm and a measured resolution of around 4.5 mm. ^{18}F-PSMA-11 was synthesized as described by Kersemans *et al.* (*14*). After IV injection of 2.0 ± 0.2 MBq ^{18}F-PSMA-11 per kg body weight, a whole-body PET scan was acquired, followed by additional imaging at 20, 50, 90 and 300 minutes after radiotracer injection. PET emission times varied from 45 seconds (scan at time of injection and 20 min p.i.), to 80 seconds (scan at 50 min p.i.) and 2 min (scan at 90 and 300 min p.i.)/bed position. Each PET scan was preceded by a low-dose CT scan (100 keV, 30 mAs) for attenuation correction. Reconstruction of the PET scans was performed using the QClear algorithm (GE Healthcare), a block sequential regularized expectation maximization algorithm (*23*). The reconstruction takes into account Time-of-Flight information, point spread function compensation, CT based attenuation and scatter correction, and a beta-parameter of 600 was chosen.

To determine the clearance rate from the blood, small venous blood samples (collected at 5, 10, 20, 30, 50, 70, 90 and 300 minutes p.i.) were measured using a calibrated gamma counter (Cobra, Packard). Additionally, patients were asked to empty the bladder before administration of the radiotracer, followed by collection of the excreted urine at 90, 180 and 300 minutes p.i. At each time point, a sample was measured using a calibrated gamma counter (Cobra, Packard).

Defluorination of ^{18}F-PSMA-11 was determined by collection of an additional blood sample at 20, 50 and 90 minutes p.i. Blood samples were centrifuged at 4000 rpm for 10 minutes at 4°C.

After collection of the supernatant, 1 mL plasma was diluted 1:5 with 0.05M acetate buffer pH 4.5 and loaded on two Oasis HLB columns in tandem which were preconditioned with 10 mL 70% ethanol and 10 mL MilliQ H_2O. Finally, the columns were washed with 2 x 4 mL MilliQ H_2O. The spill over and wash were collected and activity was measured using a calibrated gamma counter (Cobra, Packard) as these fractions represent the free fraction of ^{18}F-fluoride. The results were expressed as percentage free ^{18}F-fluoride.

Based on the fused PET/CT data, volumes of interest of bone, liver, kidneys, spleen, lacrimal glands, parotis glands, submandibular glands, aortic arch, pancreas, lungs, brain, and total body were manually delineated using the Mirada Simplicit^{90}Y^{TM} software build 1.1.0.26641 (MIRADA Medical, Oxford, UK). To examine the biodistribution of the radiotracer, time-activity curves (TACs) were calculated by determining the radioactivity concentration for each organ, correcting it for decay, and plotting it versus time. Subsequently, a time-integrated activity coefficient was determined for each organ by fitting the TACs with a one or bi-exponential function using SPSS version 25. Internal organ doses calculations were performed with IDAC dose 2.1 software. The latter tool estimates the organ dose based on earlier published photon-specific absorbed fractions for the ICRP male adult reference computational voxel phantom (*24*). For the determination of the absorbed dose of the bladder, a voiding interval of 3h was taken into account. Finally, the effective dose was calculated using ICRP 103 tissue weighing factors (*25*).

RESULTS

Radiochemical purities of the final formulation were determined using thin layer chromatography and high performance liquid chromatography and exceeded 95% and 98% respectively. The mean administered mass of PSMA-11 was 2.9 ± 1.2 µg. The mean injected activity of ^{18}F-PSMA-11 was 1.91 ± 0.10 MBq/kg (mean total activity 163.5 ± 33.5 MBq).

All six patients tolerated the drug product well. No clinically relevant changes have been observed in vital parameters. Blood samples analysed for haematology and biochemistry indicated no changes larger than the test method and within-subject biological variability. The only exceptions were a high white blood cell count (grade 1 CTCAE) before administration of ^{18}F-PSMA-11 and an increase in serum creatinine levels (grade 1 CTCAE) at 5h post ^{18}F-PSMA-11 administration in patient 3. None of the patients reported any side effects.

For each patient, the activity in whole blood was plotted as percentage of the total injected radioactivity dose (%ID) as a function of time (Fig. 1). The total blood volume was estimated using the reference book method (*26*) where 1 kilogram of bodyweight corresponds to 75 mL blood. The radiotracer was rapidly cleared from the blood. At 10 minutes p.i., 20.08 ± 5.2 %ID was still present in whole blood which decreased to 10.89 ± 1.95 %ID after 30 minutes. The initial percentage free ^{18}F-fluoride in plasma of 4.2 ± 0.7% increased up to 9.7 ± 1.0%, 15.9 ± 2.0% and 22.2 ± 1.5% at 20, 50 and 90 minutes p.i., respectively. The mean cumulative activity in urine, expressed as a percentage of the total injected radioactivity dose encompassed 2.4 ± 4.0%, 16.3 ± 5.2% and 29.0 ± 5.9% at 90, 180 and 300 min p.i., respectively (Fig. 2).

Immediately after administration of ^{18}F-PSMA-11, vascular structures and kidneys could be observed (Fig. 3). Twenty minutes p.i., a physiological high tracer uptake was detected in lacrimal and salivary glands, kidneys, ureters, bladder, liver and spleen. Physiological moderate uptake was observed in the pancreas and intestines. In addition, all patients showed focal uptake in the skeleton (axial and peripheral) and four patients showed accumulation of activity in the lymph node regions (para-aortic, para-iliac and/or inguinal). One patient showed uptake in the lungs and one in the prostate region. The SUV_{mean} of focal uptake in two suspicious lymph nodes, two suspicious bone lesion and suspicious prostate are presented in Figure 4. The highest SUV_{mean} values at 50 min p.i. were observed in the prostate (6.03), followed by both bone lesions (3.59 in Th8 and 3.26 in the femur) and the lymph nodes (2.53 in the pelvis and 1.59 para-aortic). Figure 5 shows focal ^{18}F-PSMA uptake in the axial skeleton over time (20, 50 and 90 minutes post injection).

Figure 6 demonstrates the biodistribution of ^{18}F-PSMA-11 in all major contributing organs, expressed as percentage of the injected dose per gram tissue (%ID/g). The highest %ID/g were observed in kidneys and bladder (max observed values are 0.0713 %ID/g and 0.0550 %ID/g respectively). The %ID/g for all other organs did not exceed 0.015 %ID/g.

The mean total effective dose of ^{18}F-PSMA-11 was 12.8 ± 0.6 µSv/MBq which results in an effective dose of 1.792 mSv for an average person of 70 kg who was administered a dose of 2 MBq/kg bodyweight. Table 2 provides the estimated organ doses and effective doses for each patient. The highest mean tracer uptake was seen in the urinary bladder wall (0.126 ± 0.00327

mGy/MBq), the kidneys (0.0850 ± 0.0164 mGy/MBq), prostate region (0.0470 ± 0.00124 mGy/MBq) and salivary glands (0.0352 ± 0.0141 mGy/MBq). Comparison of the total effective dose and the absorbed dose per organ with other commonly used radiotracers are presented in Figure 7 and 8, respectively.

DISCUSSION

Concerning the safety of administration of ^{18}F-PSMA-11, all patients tolerated the drug product well. The only exception was a grade 1 CTCAE increase in serum creatinine levels in patient 3. It is very unlikely that this increase is related to the study drug and can more likely be attributed to the consumption of a cooked meat meal by a diabetic patient between the two blood samples (pre and post ^{18}F-PSMA-11 scan) for serum creatinine determination. This type and degree of temporary deterioration of renal function after a cooked meal has been frequently described in the literature and has been observed multiple times in this particular patient (*27*,*28*). The patient's kidney function was further monitored and recuperated well.

^{18}F-PSMA-11 demonstrates favourable radiotracer characteristics such as rapid clearance from the blood, which suggest fast distribution to tissues and elimination pathways. A high renal clearance rate can be seen after evaluation of urine samples as 29.0 ± 5.9% of the injected activity was excreted 5h post injection. This corresponds to the highest absorbed doses which were measured in the urinary bladder wall (0.126 ± 0.00327 mGy/MBq) and the kidneys (0.0850 ± 0.0164 mGy/MBq). These absorbed doses are relatively low compared to other PSMA tracers such as ^{68}Ga-PSMA-11 (0.130 mGy/MBq and 0.262 mGy/MBq (*29*), respectively) and ^{18}F-PSMA-1007

(0.0187 mGy/MBq and 0.170 mGy/MBq (*30*), respectively). ^{68}Ga-PSMA-11 shows a similar biodistribution compared to ^{18}F-PSMA-11 because of structural similarities. However, the lower positron energy of ^{18}F compared to ^{68}Ga (0.65 MeV vs 1.90 MeV) gives a lower radiation dose (*15*,*29*). In a different dosimetry study, Pfob *et al.* (*31*) reported a similar absorbed dose for ^{68}Ga-PSMA-11 as for ^{18}F-PSMA-11 (urinary bladder wall: 0.164 mGy/MBq vs 0.126 mGy/MBq; kidneys: 0.122 mGy/MBq vs 0.0850 mGy/MBq). However, these values are not directly comparable as patients received 20 mg furosemide to promote urinary excretion of the radiotracer. ^{18}F-PSMA-1007 is eliminated by hepatobiliary clearance and one would expect low absorbed doses for kidney and bladder. However, the absorbed dose for kidneys is twice as high compared to ^{18}F-PSMA-11 which is caused by retention of ^{18}F-PSMA-1007 in kidney parenchyma (*30*). Comparison of the bladder absorbed dose between these two radiotracers is more difficult, as time activity curves of ^{18}F-PSMA-1007 were corrected for renal excretion of the activity (*30*). In dosimetry calculations, a voiding interval of 3h was applied. As prostate cancer patients are known for urinary incontinence, a urinary frequency of 8 times/day is an underestimation, but ensures the estimated radiation dose represents the worst case scenario.

Figure 4 shows that the SUV_{mean} in the selected suspicious lesions remained constant over time between 20 and 90 min p.i. which suggests retention of the radiotracer in these foci. However, as no diagnostic CT scan was performed, it is difficult to evaluate the nature of the focal uptake lesions.

Measurement of the free ^{18}F-fluoride fraction in plasma indicated an increase up to 22.2 ± 1.5% 90 minutes p.i. However, this elevated fraction of ^{18}F-fluoride is not reflected in a substantial increase of the activity measured in bone as the mean percentage of bone to whole body activity increases only with 1.4% (50 vs 20 min p.i.) and 2.5% (90 vs 50 min p.i.). This can be explained by rapid plasma clearance, renal excretion of ^{18}F-fluoride and the fact that only 7.9 ± 1.6% and 3.9 ± 1.4% of the injected dose is still present in the blood at 50 and 90 min p.i. respectively. An additional calculation has been performed where the contribution of the radioactivity uptake in the bone to the total absorbed dose by the bone (endosteum) is determined by entering the bone activity as the only source organ in the IDAC dose 2.1 radiation dosimetry software. A maximum of only 14% of the absorbed dose in the endosteum can be attributed to radiotracer accumulation in the bone. While Figure 3 and 5 indicate that background activity in bone at 50 and 90 minutes is sufficiently low for identification of suspicious foci, high background noise might limit the interpretation of images acquired at 300 min post injection. Therefore, it can be estimated that the optimum time window extends from 50 to approximately 180 minutes post injection. However, defining the optimal timepoint for scanning will be a primary endpoint of the phase 2 trial.

The comparison of the defluorination rate and the absorbed bone dose between ^{18}F-PSMA-11 and other PSMA radiotracer analogues is complicated. On the one hand, not all studies applied a chromatographic technique (e.g. TLC) appropriate for the determination of the free ^{18}F-fluoride fraction in plasma. On the other hand, various radiation dosimetry software such as IDAC dose 2.1 and OLINDA/EXM were used which estimate an absorbed dose for the endosteum and the osteogenic cells, respectively. Replicating our ^{18}F-PSMA-11 dosimetry using OLINDA/EXM

(Supplemental Table 1) gives rise to an absorbed osteogenic cell dose of 0.0107 ± 0.0024 mGy/MBq, which is similar compared to ^{18}F-DCFPyl (0.00958 mGy/MBq) (*18*) and lower compared to other ^{18}F-labelled PSMA analogues such as ^{18}F-PSMA-1007 (0.0155 mGy/MBq) (*30*), and ^{18}F-DCFBC (0.0182 mGy/MBq) (*32*). Nevertheless, comparison remains difficult as not every dosimetry study incorporated bone activity as a separate source organ.

The total effective dose of ^{18}F-PSMA-11 of 12.8 µSv/MBq is similar to ^{18}F-DCFPyL (0.0139 mSv/MBq) (*18*) but lower compared to other known PSMA tracers such as ^{18}F-DCFBC (0.0199 mSv/MBq) (*32*), ^{68}Ga-PSMA-617 (0.0208 mSv/MBq) (*33*), ^{18}F-PSMA-1007 (0.022 mSv/MBq) (*30*) and ^{68}Ga-PSMA-11 (0.023 mSv/MBq) (*29*) (Fig. 7). The low effective dose of ^{18}F-PSMA-11 is attributable to high urinary clearance, low positron energy of ^{18}F and low absorbed doses for radiosensitive organs such as testes, thymus and thyroid.

Figure 8 compares the most important corresponding organ absorbed doses for the most common used PSMA PET tracers (^{18}F-DCFPyL (*18*), ^{18}F-DCFBC (*32*), ^{68}Ga-PSMA-617 (*33*), ^{18}F-PSMA-1007 (*30*), ^{68}Ga-PSMA-11 (*29*) and ^{18}F-PSMA-11). The most significant differences can be found in the absorbed dose of the kidneys, urinary bladder, liver and spleen (Supplemental Table 2).

This paper presents a comparison of the effective radiation dose between different PSMA radiotracer analogues. It should be noted that differences in used scanners, scan protocols and patient population might also have an impact on the estimated radiation doses. Furthermore, the method for detection of metabolites only focuses on the defluorination rate of ^{18}F-PSMA-11 and

did not reinvestigate the stability of the PSMA-11 molecule in the human body as Malik *et al.* (*20*) already demonstrated the stability of the PSMA-11 molecule over time in serum.

CONCLUSION

^{18}F-PSMA-11 shows rapid blood clearance and high renal excretion. The highest absorbed doses were determined for kidneys (0.0850 ± 0.0164 mGy/MBq) and bladder (0.126 ± 0.00327 mGy/MBq). ^{18}F-PSMA-11 results in a mean effective dose of 12.8 ± 0.6 µSv/MBq and has therefore a similar radiation dose of ^{18}F-DCFPyL and lower compared to other PSMA PET agents. These results make ^{18}F-PSMA-11 a feasible PET tracer for subsequent patient studies, determining scan protocol and diagnostic accuracy in prostate cancer.

ACKNOWLEDGEMENTS

The authors would like to thank the cyclotron team and nursing staff of the department nuclear medicine of Ghent University Hospital for the production of the radiotracer and the outstanding cooperation.

DISCLOSURES

No potential conflicts of interest relevant to this article exist.

KEY POINTS

This clinical study was conducted to assess the safety of administration and biodistribution of ^{18}F-PSMA-11 in humans. The mean effective dose of ^{18}F-PSMA-11 was 12.8 ± 0.6 µSv/MBq. The highest absorbed doses were determined for kidneys (0.0850 ± 0.0164 mGy/MBq) and bladder (0.126 ± 0.00327 mGy/MBq). With an effective dose lower compared to most common used PET radiotracers, patients that undergo a ^{18}F-PSMA-11 PET scan will be exposed to a lower radiation dose.

REFERENCES

1. Zhou CK, Check DP, Lortet-Tieulent J, et al. Prostate cancer incidence in 43 populations worldwide: An analysis of time trends overall and by age group. *Int J cancer*. 2016;138:1388-400.

2. Paller CJ, Antonarakis ES. Management of biochemically recurrent prostate cancer after local therapy: evolving standards of care and new directions. *Clin Adv Hematol Oncol*. 2013;11:14-23.

3. McLeod DG. The effective management of biochemical recurrence in patients with prostate cancer. *Rev Urol*. 2005;7 Suppl 5:S29-36.

4. Kosuri S, Akhtar NH, Smith M, Osborne JR, Tagawa ST. Review of salvage therapy for biochemically recurrent prostate cancer: the role of imaging and rationale for systemic salvage targeted anti-prostate-specific membrane antigen Radioimmunotherapy. *Adv Urol*. 2012;2012:1-8.

5. Eiber M, Maurer T, Souvatzoglou M, et al. Evaluation of Hybrid ^{68}Ga-PSMA Ligand PET/CT in 248 Patients with Biochemical Recurrence After Radical Prostatectomy. *J Nucl Med*. 2015;56:668-74.

6. American Urological Association (AUA). PSA Testing for the Pretreatment Staging and Posttreatment Management of Prostate Cancer. http://www.auanet.org/guidelines/prostate-specific-antigen-(2009-amended-2013).

7. Buyyounouski MK, Hanlon AL, Eisenberg DF, et al. Defining biochemical failure after radiotherapy with and without androgen deprivation for prostate cancer. *Int J Radiat Oncol*. 2005;63:1455-1462.

8. Sweat SD, Pacelli A, Murphy GP, Bostwick DG. Prostate-specific membrane antigen expression is greatest in prostate adenocarcinoma and lymph node metastases. *Urology*. 1998;52:637-40.

9. Mannweiler S, Amersdorfer P, Trajanoski S, Terrett JA, King D, Mehes G. Heterogeneity of

prostate-specific membrane antigen (PSMA) expression in prostate carcinoma with distant metastasis. *Pathol Oncol Res*. 2009;15:167-172.

10. Tian J-Y, Guo F-J, Zheng G-Y, Ahmad A. Prostate cancer: updates on current strategies for screening, diagnosis and clinical implications of treatment modalities. *Carcinogenesis*. 2018;39:307-317.

11. Roach PJ, Francis R, Emmett L, et al. The Impact of 68Ga-PSMA PET/CT on Management Intent in Prostate Cancer: Results of an Australian Prospective Multicenter Study. *J Nucl Med*. 2018;59:82-88.

12. Zacho HD, Nielsen JB, Afshar-Oromieh A, et al. Prospective comparison of 68Ga-PSMA PET/CT, 18F-sodium fluoride PET/CT and diffusion weighted-MRI at for the detection of bone metastases in biochemically recurrent prostate cancer. *Eur J Nucl Med Mol Imaging*. June 2018:1-14.

13. Mottet N, Bellmunt J, Bolla M, et al. EAU-ESTRO-SIOG guidelines on prostate cancer. Part 1: screening, diagnosis, and local treatment with curative intent. *Eur Urol*. 2017;71:618-629.

14. Kersemans K, De Man K, Courtyn J, et al. Automated radiosynthesis of Al[18 F]PSMA-11 for large scale routine use. *Appl Radiat Isot*. 2018;135:19-27.

15. Kesch C, Kratochwil C, Mier W, Kopka K, Giesel FL. 68 Ga or 18 F for prostate cancer imaging? *J Nucl Med*. 2017;58:687-688.

16. Sanchez-Crespo A. Comparison of Gallium-68 and Fluorine-18 imaging characteristics in positron emission tomography. *Appl Radiat Isot*. 2013;76:55-62.

17. Rowe SP, Gage KL, Faraj SF, et al. ^{18}F-DCFBC PET/CT for PSMA-based detection and characterization of primary prostate cancer. *J Nucl Med*. 2015;56:1003-1010.

18. Szabo Z, Mena E, Rowe SP, et al. Initial evaluation of [(18)F]DCFPyL for prostate-specific

membrane antigen (PSMA)-targeted PET imaging of prostate cancer. *Mol Imaging Biol*. 2015;17:565-74.

19. Cardinale J, Schäfer M, Benešová M, et al. Preclinical evaluation of18F-PSMA-1007, a new prostate-specific membrane antigen ligand for prostate cancer imaging. *J Nucl Med*. 2017;58:425-431.

20. Malik N, Baur B, Winter G, Reske SN, Beer AJ, Solbach C. Radiofluorination of PSMA-HBED via Al18F2+ Chelation and Biological Evaluations In Vitro. *Mol Imaging Biol*. 2015;17:777-785.

21. Boschi S, Lee JT, Beykan S, et al. Synthesis and preclinical evaluation of an Al 18 F radiofluorinated GLU-UREA-LYS (AHX) -HBED-CC PSMA ligand. *Eur J Nucl Med Mol Imaging*. 2016:2122-2130.

22. Giglio J, Zeni M, Savio E, Engler H. Synthesis of an Al18F radiofluorinated GLU-UREA-LYS(AHX)-HBED-CC PSMA ligand in an automated synthesis platform. *EJNMMI Radiopharm Chem*. 2018;3:4.

23. Ahn S, Fessler JA. Globally convergent image reconstruction for emission tomography using relaxed ordered subsets algorithms. *IEEE Trans Med Imaging*. 2003;22:613-626.

24. Andersson M, Johansson L, Eckerman K, Mattsson S. IDAC-Dose 2.1, an internal dosimetry program for diagnostic nuclear medicine based on the ICRP adult reference voxel phantoms. *EJNMMI Res*. 2017;7:88.

25. ICRP. ICRP Publication 103: The 2007 Recommendations of the International Commission on Radiological Protection. http://www.icrp.org/publication.asp?id=ICRP Publication 103.

26. Jia ZS, Xie HX, Yang J, et al. Total blood volume of Asian patients undergoing cardiac surgery is far from that predicted by conventional methods. *J Cardiovasc Surg (Torino)*. 2013;54:423-30.

27. Nair S, O'Brien S V., Hayden K, et al. Effect of a cooked meat meal on serum creatinine and estimated glomerular filtration rate in diabetes-related kidney disease. *Diabetes Care*.

2014;37:483-487.

28. Halma C. Het serumcreatininegehalte als maat voor de nierfunctie. Nederlands Tijdschrift voor Geneeskunde. https://www.ntvg.nl/artikelen/het-serumcreatininegehalte-als-maat-voor-de-nierfunctie/volledig.

29. Afshar-Oromieh A, Hetzheim H, Kübler W, et al. Radiation dosimetry of 68Ga-PSMA-11 (HBED-CC) and preliminary evaluation of optimal imaging timing. *Eur J Nucl Med Mol Imaging*. 2016;43:1611-1620.

30. Giesel FL, Hadaschik B, Cardinale J, et al. F-18 labelled PSMA-1007: biodistribution, radiation dosimetry and histopathological validation of tumor lesions in prostate cancer patients. *Eur J Nucl Med Mol Imaging*. 2017;44:678.

31. Pfob CH, Ziegler S, Graner FP, et al. Biodistribution and radiation dosimetry of68Ga-PSMA HBED CC—a PSMA specific probe for PET imaging of prostate cancer. *Eur J Nucl Med Mol Imaging*. 2016;43:1962-1970.

32. Cho SY, Gage KL, Mease RC, et al. Biodistribution, tumor detection, and radiation dosimetry of 18F-DCFBC, a low-molecular-weight inhibitor of prostate-specific membrane antigen, in patients with metastatic prostate cancer. *J Nucl Med*. 2012;53:1883-91.

33. Afshar-Oromieh A, Hetzheim H, Kratochwil C, et al. The theranostic PSMA ligand PSMA-617 in the diagnosis of prostate cancer by PET/CT: biodistribution in humans, radiation dosimetry, and first evaluation of tumor lesions. *J Nucl Med*. 2015;56:1697-1705.

Figure 1: Time-activity curves in whole blood expressed as percentage of the total injected radioactivity dose (%ID) in function of time

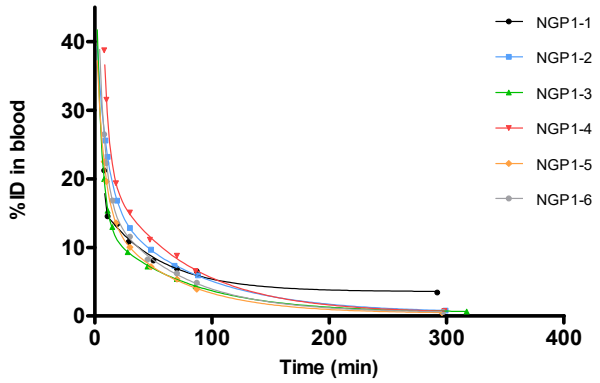

Figure 2: Mean cumulative activity in urine, expressed as percentage of the total injected radioactivity dose

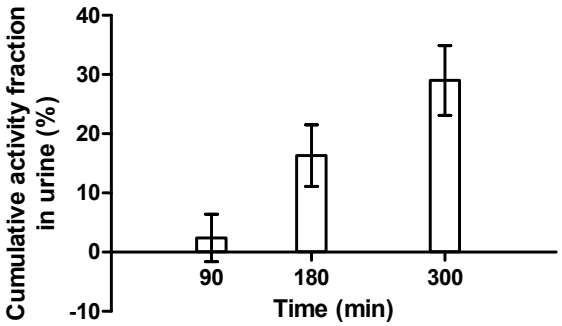

Figure 3: Overview of MIP images at 0, 20, 50, 90 and 300 minutes post injection

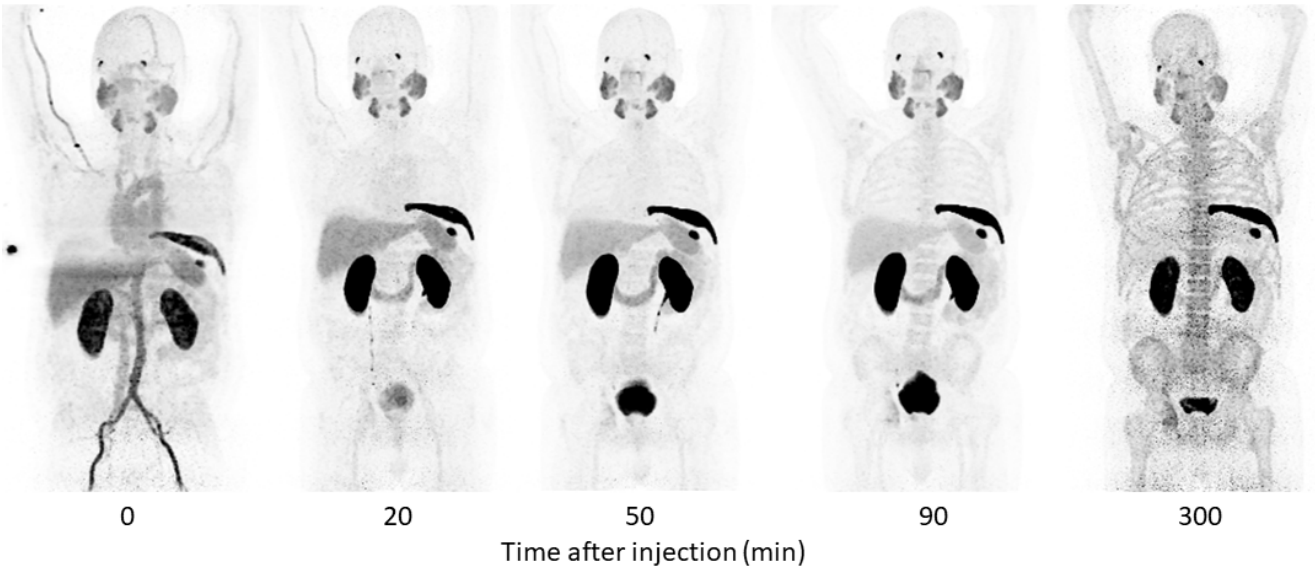

Figure 4: SUVmean values over time (20, 50 and 90 minutes p.i.) for five suspicious lesions

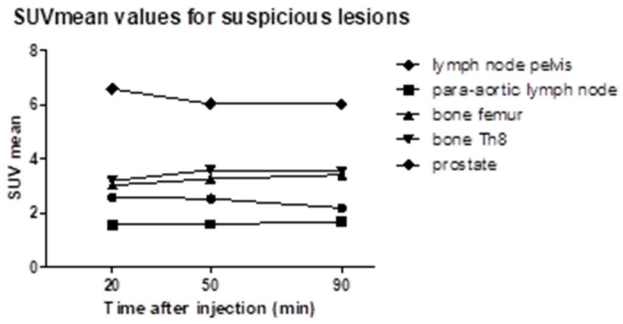

Figure 5: PET/$CT_{low\text{-}dose}$ saggital images of bone window. Two possible bone lesions can be detected at Th6 and Th8, as well as local recurrence in the prostate bed.

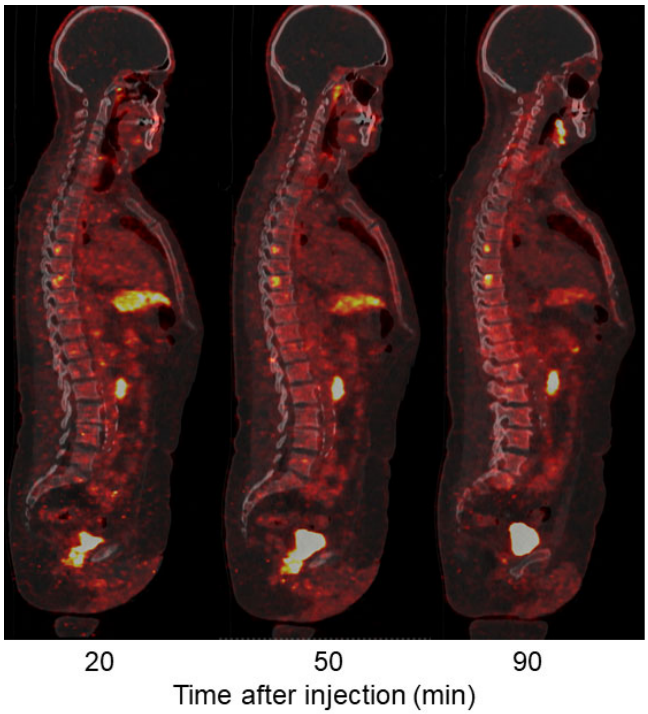

Figure 6: Time activity curve of Patient 5, expressed as the percentage of injected dose per gram tissue for all major contributing organs as a function of time

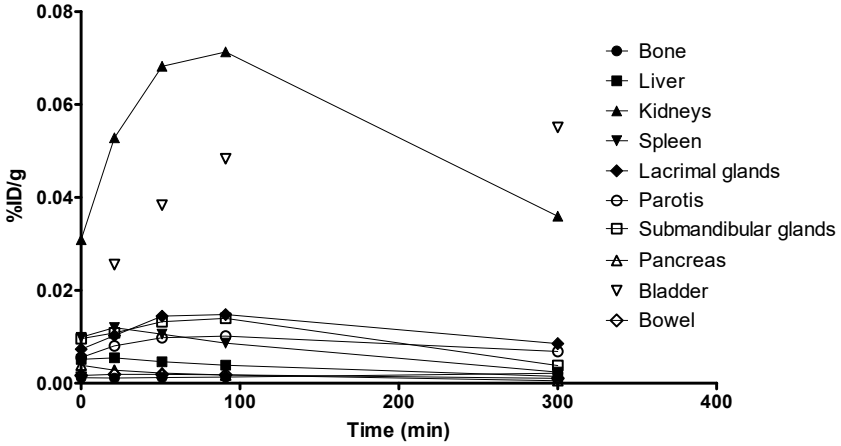

Figure 7: Comparison of mean effective doses of various recently developed PSMA PET-radiotracers

(1) Szabo et al, 2015 (2) Cho et al, 2012 (3) Afshar-Oromieh et al, 2015 (4) Giesel et al, 2017 (5) Afshar-Oromieh, 2017

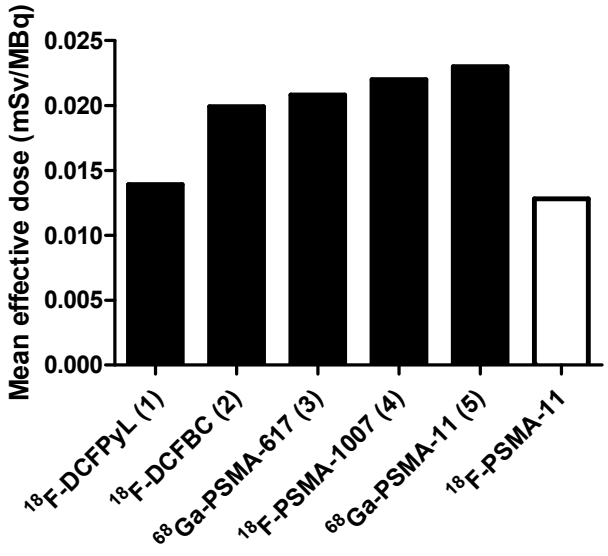

Figure 8: comparison of absorbed dose per organ for various PSMA PET tracers

(1) Szabo et al, 2015 (2) Cho et al, 2012 (3) Afshar-Oromieh et al, 2015 (4) Giesel et al, 2017 (5) Afshar-Oromieh, 2017

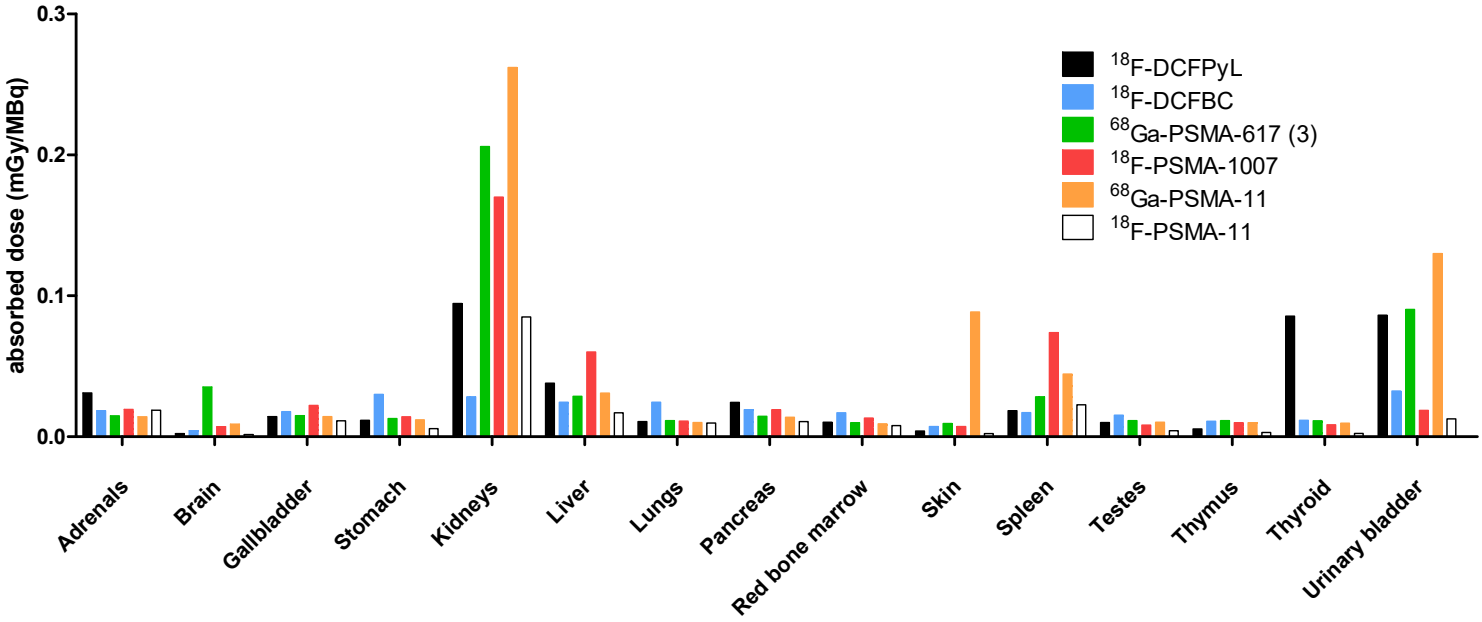

Tables

Table 1: patient characteristics

Pat no.	Age (y)	Weight (kg)	PSA-value	Gleason score	Medical history
1	67	56	0,3	7 (4+3)	Radical prostatectomy
2	67	114	1,1	5 (2+3)	Primary radiotherapy
3	68	90	42,5	7 (3+4)	Radical prostatectomy + postoperative radiotherapy and salvage lymph node dissection
4	66	99	19,0	9 (4+5)	Pelvic lymph node dissection + primary radiotherapy + androgen deprivation therapy. Castration resistant prostate cancer with rising PSA under abiraterone 1000 mg/d and prednisone 5mg 2/d.
5	66	81	5,0	7 (4+3)	Radical prostatectomy, adjuvant radiotherapy at prostate bed
6	62	80	0,5	9 (4+5)	Radical prostatectomy, radiotherapy, androgen deprivation therapy

Table 2: Estimated organ doses and effective dose using IDAC Dose 2.1

Organs [mGy/MBq]	NGP1-1	NGP1-2	NGP1-3	NGP1-4	NGP1-5	NGP1-6	mean	SD
Adrenals	1,39E-02	2,38E-02	1,81E-02	1,83E-02	1,97E-02	1,92E-02	1,88E-02	3,18E-03
Brain	1,71E-03	1,65E-03	1,35E-03	1,62E-03	1,69E-03	1,55E-03	1,60E-03	1,33E-04
Bronchi total	2,29E-02	2,89E-02	2,29E-02	2,16E-02	2,05E-02	2,18E-02	2,31E-02	2,98E-03
Colon wall	9,58E-03	1,13E-02	9,47E-03	9,72E-03	1,00E-02	1,00E-02	1,00E-02	6,67E-04
Endosteum (bone surface)	4,94E-03	5,65E-03	4,34E-03	4,90E-03	4,70E-03	4,77E-03	4,88E-03	4,32E-04
Gallbladder wall	9,99E-03	1,47E-02	1,25E-02	1,01E-02	1,03E-02	1,11E-02	1,14E-02	1,85E-03
Heart wall	4,46E-03	6,19E-03	4,63E-03	4,24E-03	4,20E-03	4,39E-03	4,69E-03	7,54E-04
Kidneys	5,78E-02	1,06E-01	7,66E-02	8,69E-02	9,28E-02	8,97E-02	8,50E-02	1,64E-02
Left colon wall	4,26E-03	6,21E-03	4,52E-03	4,52E-03	4,80E-03	4,69E-03	4,83E-03	6,99E-04
Liver	1,45E-02	2,18E-02	2,01E-02	1,47E-02	1,48E-02	1,66E-02	1,71E-02	3,14E-03
Lung	9,81E-03	1,21E-02	9,88E-03	9,28E-03	8,75E-03	9,35E-03	9,86E-03	1,17E-03
Lymph nodes total	2,70E-02	3,07E-02	2,42E-02	2,56E-02	2,53E-02	2,65E-02	2,66E-02	2,38E-03
Muscle	4,27E-03	5,08E-03	3,70E-03	4,06E-03	3,99E-03	4,05E-03	4,19E-03	4,72E-04
Pancreas	1,37E-02	1,19E-02	1,07E-02	9,20E-03	9,36E-03	9,91E-03	1,08E-02	1,74E-03
Prostate	4,76E-02	4,68E-02	4,48E-02	4,68E-02	4,81E-02	4,81E-02	4,70E-02	1,24E-03
Recto-sigmoid colon wall	2,75E-02	2,74E-02	2,58E-02	2,70E-02	2,77E-02	2,77E-02	2,72E-02	7,25E-04
Red (active) bone marrow	7,79E-03	8,98E-03	7,38E-03	7,90E-03	7,80E-03	7,90E-03	7,96E-03	5,36E-04
Right colon wall	5,93E-03	8,24E-03	6,27E-03	6,27E-03	6,38E-03	6,51E-03	6,60E-03	8,26E-04
Salivary glands	5,09E-02	3,25E-02	1,69E-02	3,27E-02	2,56E-02	5,28E-02	3,52E-02	1,41E-02
Skin	2,39E-03	3,00E-03	1,96E-03	2,18E-03	2,11E-03	2,17E-03	2,30E-03	3,69E-04
Small intestine wall	1,15E-02	1,30E-02	1,12E-02	1,16E-02	1,20E-02	1,20E-02	1,19E-02	6,27E-04
Spleen	1,26E-02	2,76E-02	3,25E-02	1,50E-02	2,84E-02	2,01E-02	2,27E-02	8,01E-03
Stomach wall	5,00E-03	7,39E-03	5,92E-03	5,11E-03	5,47E-03	5,48E-03	5,73E-03	8,76E-04
Testes	4,48E-03	5,01E-03	3,65E-03	4,04E-03	4,02E-03	4,05E-03	4,21E-03	4,73E-04
Thymus	3,21E-03	4,09E-03	2,72E-03	2,94E-03	2,67E-03	2,86E-03	3,08E-03	5,30E-04
Thyroid	2,61E-03	3,24E-03	1,95E-03	2,29E-03	2,05E-03	2,26E-03	2,40E-03	4,70E-04
Urinary bladder wall	1,27E-01	1,23E-01	1,21E-01	1,25E-01	1,29E-01	1,29E-01	1,26E-01	3,27E-03
Remainder	5,52E-02	6,32E-02	4,82E-02	5,30E-02	5,04E-02	5,37E-02	5,40E-02	6,07E-03
Effective dose[mSv/MBq]	1,26E-02	1,41E-02	1,24E-02	1,24E-02	1,26E-02	1,28E-02	1,28E-02	6,46E-04

Supplemental data

1. Supplementary Table 1: Dosimetry of [^{18}F]PSMA-11 using OLINDA/EXM

10^(-3) mGy/MBq	NGP1-1	NGP1-2	NGP1-3	NGP1-4	NGP1-5	NGP1-6	Mean	SD
Adrenals	8,32	12,7	9,9	9,82	9,88	10,1	10,1	1,4
Brain	1,86	2,13	1,81	1,82	1,86	1,89	1,9	0,1
Breasts	3,64	5,21	3,83	3,92	3,73	3,92	4,0	0,6
gallbladder wall	8,95	13,2	10,4	9,64	9,32	10,2	10,3	1,5
LLI wall	39,4	49,5	35,4	34,5	31	42,1	38,7	6,6
small intestine	8,09	11,4	8,25	8,37	7,98	9,03	8,9	1,3
stomach wall	6,29	9,25	7,05	6,82	6,9	7,13	7,2	1,0
ULI wall	28,4	36,3	26,2	25,5	23,1	30,6	28,4	4,7
heart wall	5,55	7,94	6,02	5,97	5,7	6,02	6,2	0,9
kidneys	80,7	149	108	123	131	127	119,8	23,3
liver	17,6	26	24,6	17,7	16,6	19,6	20,4	4,0
lungs	13,6	17,3	13,7	14	12,1	13,4	14,0	1,7
muscle	4,59	6,61	4,86	5,03	4,85	5,1	5,2	0,7
pancreas	18,6	13,3	11,6	10,4	10,9	11,4	12,7	3,1
red marrow	5,23	7,23	5,54	5,88	5,65	5,89	5,9	0,7
osteogenic cells	11,5	9,07	8,15	13,9	12,8	8,74	10,7	2,4
skin	3,27	4,71	3,43	3,59	3,45	3,6	3,7	0,5
spleen	15,2	35,2	41,9	19	36,4	25,7	28,9	10,6
testes	6,48	5,47	3,84	4,1	8,13	4,12	5,4	1,7
thymus	4,36	6,23	4,52	4,71	4,46	4,68	4,8	0,7
thyroid	3,89	5,52	3,96	4,24	1,03	4,18	3,8	1,5
urinary bladder wall	5,2	7,38	5,2	5,46	5,19	5,62	5,7	0,9
uterus	5,97	8,48	6,02	6,28	5,97	6,53	6,5	1,0
total body	5,77	8,22	6,36	6,42	6,22	6,55	6,6	0,8
effective dose (mSv/MBq)	0,0132	0,0185	0,0124	0,0139	0,0114	0,0151	0,014	0,003

2. Supplementary Table 2: Comparison of absorbed doses of various organs for the most common used PSMA PET tracers. The colour scale shows the reported doses per organ from the lowest dose (dark blue) to the highest dose (dark red).

Organs (mGy/MBq)	[^{18}F]DCFBC Cho et al., 2012	[^{18}F]DCFPyL Szabo et al., 2015	[^{68}Ga]PSMA 617 Afshar-Oromieh et al., 2015	[^{18}F]PSMA 1007 Giesel et al., 2017	[^{68}Ga]PSMA 11 Afshar-Oromieh et al., 2017	[^{18}F]PSMA-11 Piron et al.
Adrenals	1,85E-02	3,11E-02	1,48E-02	1,94E-02	1,42E-02	1,88E-02
Brain	4,21E-03	2,19E-03	3,53E-02	7,20E-03	9,00E-03	1,60E-03
Gallbladder wall	1,79E-02	1,44E-02	1,50E-02	2,22E-02	1,44E-02	1,14E-02
LLI wall[1]	2,47E-02	1,05E-02	1,33E-02	4,83E-02	1,23E-02	4,83E-03
Small intestine	2,36E-02	9,13E-03	1,83E-02	1,56E-02	1,63E-02	1,19E-02
Stomach wall	3,02E-02	1,16E-02	1,30E-02	1,42E-02	1,20E-02	5,73E-03
ULI wall[2]	2,34E-02	1,67E-02	4,48E-02	4,08E-02	5,40E-02	6,60E-03
Heart wall	2,92E-02	1,29E-02	1,20E-02	2,51E-02	1,09E-02	4,69E-03
Kidneys	2,84E-02	9,45E-02	2,06E-01	1,70E-01	2,62E-01	8,50E-02
Liver	2,46E-02	3,80E-02	2,88E-02	6,02E-02	3,09E-02	1,71E-02
Lungs	2,45E-02	1,08E-02	1,15E-02	1,11E-02	1,02E-02	9,86E-03
Muscle	9,69E-03	6,32E-03	1,15E-02	1,00E-02	1,05E-02	4,19E-03
Pancreas	1,92E-02	2,44E-02	1,45E-02	1,92E-02	1,38E-02	1,08E-02
Red marrow	1,70E-02	1,04E-02	1,00E-02	1,33E-02	9,20E-03	7,96E-03
Skin	7,30E-03	4,05E-03	9,50E-03	7,30E-03	8,85E-02	2,30E-03
Spleen	1,72E-02	1,85E-02	2,85E-02	7,39E-02	4,46E-02	2,27E-02
Testes	1,54E-02	1,01E-02	1,15E-02	8,37E-03	1,04E-02	4,21E-03
Thymus	1,10E-02	5,56E-03	1,15E-02	9,90E-03	9,90E-03	3,08E-03
Thyroid	1,17E-02	8,56E-02	1,13E-02	8,50E-03	9,70E-03	2,40E-03
Urinary bladder wall	3,24E-02	8,64E-02	9,03E-02	1,87E-02	1,30E-01	1,26E-02
Effective dose (mSv/MBq)	1,99E-02	1,39E-02	2,08E-02	2,20E-02	2,36E-02	1,28E-02

[1] lower large intestinal wall, [2] upper large intestinal wall